Margien G.S. Boels,[1] M. Cristina Avramut,[2] Angela Koudijs,[1]
Martijn J.C. Dane,[1] Dae Hyun Lee,[1] Johan van der Vlag,[3] Abraham J. Koster,[2]
Anton Jan van Zonneveld,[1] Ernst van Faassen,[1] Hermann-Josef Gröne,[4]
Bernard M. van den Berg,[1] and Ton J. Rabelink[1]

Atrasentan Reduces Albuminuria by Restoring the Glomerular Endothelial Glycocalyx Barrier in Diabetic Nephropathy

Diabetes 2016;65:2429–2439 | DOI: 10.2337/db15-1413

Atrasentan, a selective endothelin A receptor antagonist, has been shown to reduce albuminuria in type 2 diabetes. We previously showed that the structural integrity of a glomerular endothelial glycocalyx is required to prevent albuminuria. Therefore we tested the potential of atrasentan to stabilize the endothelial glycocalyx in diabetic apolipoprotein E (apoE)–deficient mice in relation to its antialbuminuric effects. Treatment with atrasentan (7.5 mg/kg/day) for 4 weeks reduced urinary albumin-to-creatinine ratios by 26.0 ± 6.5% ($P < 0.01$) in apoE knockout (KO) mice with streptozotocin-induced diabetes consuming an atherogenic diet, without changes in gross glomerular morphology, systemic blood pressure, and blood glucose concentration. Endothelial cationic ferritin surface coverage, investigated using large-scale digital transmission electron microscopy, revealed that atrasentan treatment increases glycocalyx coverage in diabetic apoE KO mice from 40.7 ± 3.2% to 81.0 ± 12.5% ($P < 0.05$). This restoration is accompanied by increased renal nitric oxide concentrations, reduced expression of glomerular heparanase, and a marked shift in the balance of M1 and M2 glomerular macrophages. In vitro experiments with endothelial cells exposed to laminar flow and cocultured with pericytes confirmed that atrasentan reduced endothelial heparanase expression and increased glycocalyx thickness in the presence of a diabetic milieu. Together these data point toward a role for the restoration of endothelial function and tissue homeostasis through the antialbuminuric effects of atrasentan, and they provide a mechanistic explanation for the clinical observations of reduced albuminuria with atrasentan in diabetic nephropathy.

End-stage renal disease is inevitable in a majority of patients with diabetic nephropathy (1), despite optimal blood pressure treatment using drugs that interfere with the renin-angiotensin system. Therefore there is a great need for additional strategies to slow the progression of chronic kidney disease in patients with diabetic nephropathy. One such strategy involves interaction with the endothelin (ET) system. Numerous studies involving experimental animal models have implicated ET in the pathogenesis of diabetic nephropathy (2). Moreover, clinical studies show promise for ET receptor antagonists in the treatment of diabetic nephropathy (3–6). This is particularly true for selective ET_A receptor blockers; ET_A receptor signaling seems to be involved in key renal pathophysiological processes such as the inflammatory response of renal epithelium to albumin (7), whereas stimulation of the associated concomitant ET_B receptor can restore endothelial dysfunction by inducing endothelial nitric oxide (NO) production (8–10). Because actual loss of renal function is a late indicator of disease, albuminuria has been put forward as a sensitive surrogate marker for ongoing renal injury in diabetic nephropathy. In this respect ET_A receptor blockers seem to have a striking

[1]Einthoven Laboratory for Experimental Vascular Medicine, Department of Nephrology, Leiden University Medical Center, Leiden, the Netherlands
[2]Department of Molecular Cell Biology, Leiden University Medical Center, Leiden, the Netherlands
[3]Department of Nephrology, Radboud Institute for Molecular Life Sciences, Radboud University Medical Center, Nijmegen, the Netherlands
[4]Department of Cellular and Molecular Pathology, German Cancer Research Center, Heidelberg, Germany

Corresponding author: Margien G.S. Boels, m.g.s.boels@lumc.nl.

Received 12 October 2015 and accepted 20 March 2016.

This article contains Supplementary Data online at http://diabetes.diabetesjournals.org/lookup/suppl/doi:10.2337/db15-1413/-/DC1.

See accompanying article, p. 2115.

antiproteinuric effect that cannot be fully explained by reduced blood pressure (11).

We and others previously demonstrated that maintenance of the structural integrity of a glomerular endothelial glycocalyx is crucial to prevent albuminuria (12,13). The endothelial glycocalyx is a gel-like, polyanionic carbohydrate layer that covers endothelial cells. The glomerular fenestrae appear to be densely filled with the carbohydrate polymer hyaluronan, and its enzymatic removal greatly enhances albumin passage across the glomerular filtration barrier (13). Increased activity of both heparanase and hyaluronidase reduces the dimensions of the glomerular endothelial glycocalyx and has long been recognized in diabetic nephropathy (14). Also increased circulating levels of hyaluronan have been measured in patients with diabetic nephropathy (15).

We therefore hypothesized that a selective ET_A receptor blockade confers antialbuminuric and renoprotective effects by restoring the endothelial glycocalyx barrier against albumin filtration. To this end, we examined the renoprotective effects of orally administrated atrasentan, a selective ET_A receptor blocker (16), in a diabetic nephropathy model using apolipoprotein E knockout (apoE KO) mice. This model combines renal and vascular injury with both hyperglycemia and hyperlipidemia, thus mimicking features of diabetic nephropathy (17,18); moreover, it has been shown that the model can be used for pharmacological intervention studies, including studies of ET blockers (17). In this study we show that atrasentan improves endothelial function and results in almost complete restoration of the endothelial glycocalyx while it concomitantly reduces albuminuria. In vitro analysis shows that this effect of atrasentan can be mediated through the reduction of endothelial heparanase expression.

RESEARCH DESIGN AND METHODS

Diabetic ApoE KO Mouse Model

Six-week-old male apoE KO mice (The Jackson Laboratory, Bar Harbor, ME) were rendered diabetic by intraperitoneal injections of streptozotocin (STZ) (Sigma-Aldrich, St. Louis, MO) in citrate buffer at a dose of 60 mg/kg for 5 consecutive days (19,20). Control apoE KO mice received citrate buffer alone, were fed a diet of chow, and used for baseline measurements. Only animals with average blood glucose concentrations >20 mmol/L 2 weeks after the induction of diabetes were included in the study. Twelve weeks after induction of diabetes, mice were further randomized into two groups: *1*) nontreated mice and *2*) mice treated with atrasentan (7.5 mg/kg/day via drinking water; AbbVie, North Chicago, IL) for 4 weeks. Concentrations of atrasentan in drinking water were adjusted weekly based on the preceding intake to adjust for the short half-life of atrasentan in mice. All diabetic animals had free access to cholesterol-enriched (0.15%) chow (Technilab-BMI, Someren, the Netherlands). Animal experiments were approved by the Ethical Committee on Animal Care and Experimentation at the Leiden University Medical Center (Leiden, the Netherlands). All work with animals was performed in compliance with the Dutch government's guidelines.

Blood glucose concentrations were measured using a glucose meter (Accu-Chek; Roche, Basel, Switzerland). When concentrations exceeded 25 mmol/L, mice were treated with 1–2 U insulin (Lantus; Aventis Pharmaceuticals, Bridgewater, NJ) for a maximum of three times per week. Systolic blood pressure was assessed using the CODA noninvasive tail cuff system (Kent Scientific, Torrington, CT) in conscious mice at the beginning, middle, and end of treatment. Animals were habituated to the device before measurements.

Urine Collection and Analyses

Urine was collected (via the 24-h urine test) at the start of the study period and after 2 and 4 weeks of treatment. Mice were acclimatized to metabolic cages, after which 24-h urine was collected. Urine was centrifuged to remove debris and stored at −20°C. Albumin concentrations were quantified with Rocket immunoelectrophoresis using the protocol described by Tran et al. (21), with modifications. Urine creatinine concentrations were determined by the Jaffé method using 0.13% picric acid (Sigma-Aldrich) and were quantified using a creatinine standard set (Sigma-Aldrich). Excretion of 24-h urinary kidney injury molecule-1 (KIM-1) was determined with an ELISA kit (R&D Systems, Minneapolis, MN). Optical densities for creatinine and KIM-1 were measured with an ELISA plate reader.

Determination of Glomerular Endothelial Glycocalyx Coverage

We identified glomerular areas of the endothelial glycocalyx in two ways. First, for electron microscopic visualization of the glycocalyx, three mice per group were anesthetized (intraperitoneally) with a cocktail of midazolam (1 mg/mL; Roche), dexmedetomidine (50 μg/mL; Orion Corporation, Espoo, Finland), and fentanyl (10 μg/mL; Hameln Pharmaceuticals GmbH, Hameln, Germany) in water. The abdominal aorta was exposed and cannulated adjacent to the left renal artery. The right renal artery was ligated at the renal stalk. The left kidney was perfused with 0.5% BSA and 5 U/mL heparin in 5 mL HEPES-buffered salt solution (HBSS) at 2 mL/min to remove blood, followed by 2 mL of cationic ferritin (horse spleen, 2.5 mg/mL; Electron Microscopy Sciences, Fort Washington, PA) in HBSS alone at 2 mL/min. This kidney was excised, and the capsule was removed and stored in a fixative (1.5% glutaraldehyde + 1% paraformaldehyde in 0.1 M sodium-cacodylate–buffered solution [pH 7.4]) overnight at 4°C. The kidney was subsequently sectioned in 180-μm-thick sections, rinsed with 0.1 M sodium-cacodylate–buffered solution, and fixed in 1% osmium tetroxide and 1.5% potassium ferrocyanide in ultrapure water. Samples were dehydrated, stained, and embedded in Epon LX-112. Sections (100 nm) were mounted on copper slot grids and further stained with 7% uranyl acetate and Reynold's lead citrate. Transmission electron microscopy (TEM) data were collected at an acceleration voltage of 120 kV on a Tecnai G^2 Spirit BioTWIN microscope (FEI, Eindhoven, the Netherlands), equipped with an FEI Eagle charge-coupled device camera. To create

an overview of the glomerulus, albeit with a high resolution, images with ×18,500 magnification at the detector plane, corresponding to a 1.2-nm pixel size at the specimen level, were automatically combined with stitching software (22). The resulting large digital image provides an overview of the glomerulus, which one can zoom in to view high detail, allowing for quantitative analyses. The polyanionic glycocalyx on the surface of endothelial cells can be visualized in TEM through the binding of electron-dense cationic substances such as cationic ferritin to it (23). Within the stitches, individual capillary loops were captured and glycocalyx coverage was quantified in 6–11 capillary loops in three glomeruli per mouse (n = 3/group). The percentage of positive coverage of the endothelium with cationic ferritin was determined using an automatic grid overlay in the public domain (ImageJ, version 1.46; National Institutes of Health, Bethesda, MD). For every glomerulus, a minimum of 80 crosshairs were at the intersection of the endothelium and scored for percentage positive.

Second, endothelial glycocalyx coverage was also determined using fluorescently labeled lectin, as described previously (13). In short, 100-μm sections of nonperfused kidneys of three mice per group were incubated with 10 mg/mL of fluorescently labeled *Lycopersicon esculentum* (LEA) to visualize the glycocalyx, in combination with 5 mg/mL monoclonal mouse anti-mouse CD31 antibody (Santa Cruz Biotechnology, Santa Cruz, CA) to identify the endothelial cell membrane. Next, slices were incubated for 1 h with 10 mg/mL Alexa Fluor-568–conjugated goat anti-mouse IgG (Molecular Probes, Grand Island, NY) and Hoechst 33528 (Sigma-Aldrich, 1/1,000). The amount of endothelial glycocalyx was quantified by calculating the distance from the peak of the CD31 signal to the half-width of the intraluminal lectin signal along a line of interest, using intensity profiles in ImageJ software.

Immunohistochemistry and Morphometric Analysis

Eight mice per treatment group were anesthetized by isoflurane inhalation and perfused via the left ventricle with HBSS containing 0.5% BSA and 5 U/mL heparin to remove blood. Kidneys were excised and cut in half after removing the capsules. One half was fixed in paraformaldehyde solution (4%) for 1–2 h, then was embedded in paraffin for periodic acid Schiff and trichrome staining and podocyte and macrophage quantification. The other half was snap-frozen in 2-methylbutane (Sigma-Aldrich) for immunohistochemistry. Frozen kidney sections (4 μm thick) were fixed in acetone for 10 min at room temperature. Nonspecific antibody binding was prevented by incubation with normal goat serum (4%) in PBS for 30 min. Heparanase expression was detected after overnight incubation with primary antibody (polyclonal rabbit anti-heparanase 1.5 μg/mL; InSight Biopharmaceuticals, Rehovot, Israel), followed by incubation with goat anti-rabbit IgG–Alexa 594 (1/1,000) for 1 h, both in blocking buffer. Sections were counterstained with Hoechst (1/1,000) and embedded in Vectashield mounting medium (Vector Laboratories, Inc., Burlingame, CA). Cathepsin-L polyclonal antibody (R&D Systems) was incubated overnight, followed by horseradish peroxidase–conjugated secondary antibody and 3,3′-diaminobenzidine. Heparanase and cathepsin-L staining was quantified as the percentage of stained area divided by the glomerular area.

Podocytes were quantified after being identified with Wilms' tumor-1 antibody (0.5 μg/mL; Santa Cruz Biotechnology). Macrophages were identified using a rat monoclonal antibody against mouse F4/80 (Abcam, Cambridge, MA) and a rabbit monoclonal anti-CD206 (Abcam). F4/80 recognizes a glycoprotein on the surface of most mouse macrophages (24), whereas CD206 is solely expressed by M2 macrophages (25).

Thickness of the glomerular basement membrane (GBM) was analyzed in the cationic ferritin–stained glomeruli of three mice per group using a similar grid overlay with 15 crosshairs at the intersection of the endothelium where thickness was measured. In every glomerulus eight capillary loops were analyzed for thickness of the GBM.

NO Determination

Endogenous renal NO bioavailability was measured in eight mice per treatment group using an in vivo trapping method with iron-diethyldithiocarbamate (Fe^{2+}-DETC) complexes. After anesthesia was induced (intraperitoneally, as previously described), mice were injected consecutively with iron-citrate (subcutaneously) and sodium diethyldithiocarbamate salt (intraperitoneally). When it comes in contact with free NO radicals, Fe^{2+}-DETC instantly precipitates, and detection of the resulting paramagnetic ferrous mononitrosyl-iron complex (MNIC) allows for highly specific and quantitative detection of basal (i.e., unstimulated) and elevated NO concentrations in various tissues (26–28). After 30 min of incubation, mice were killed and the organs excised. Freshly extracted renal tissue (~350 mg) was submerged in strong HEPES buffer (150 mmol/L, pH 7.4) to a total volume of 450 μL, then snap-frozen in liquid nitrogen for electron paramagnetic resonance (EPR) spectroscopy.

EPR spectra were measured at 77 K with an X-band EMX-Plus spectrometer (Bruker BioSpin, Rheinstetten, Germany). Spectrometer settings were microwave power, 20 mW; time constant, 82 ms; analog-to-digital conversion time, 82 ms; and detector gain, 10^4. The magnetic field was modulated at a frequency of 100 kHz and a 5-G amplitude. During experiments, the inside of the EPR cavity (ER4119 HS-W1, cylindrical TE_{011} mode; Bruker) was continuously flushed with dry nitrogen to prevent condensation of ambient humidity on the cool Dewar flask.

The MNIC yields in the tissue sections were quantified by comparison with frozen reference samples of paramagnetic NO-Fe^{2+}-*N*-methyl-D-glucamine dithiocarbamate complexes (10 μmol/L in PBS), in which NO concentrations could be quantified. This procedure achieves an absolute accuracy of about 10%. The lower detection limit in our setup was 40 pmol MNIC.

Coculture of Human Umbilical Vein Endothelial Cells and Human Brain Pericytes Under Flow

Coculture experiments were performed using an Ibidi flow system (Ibidi GmbH, Marensried, Germany). Freshly isolated human umbilical vein endothelial cells (HUVECs) were cultured on 0.5% gelatin–coated plastic flasks in endothelial basal medium (CC-3121; Lonza, Basel, Switzerland), supplemented with human epidermal growth factor, vascular endothelial growth factor, human fibroblast growth factor-B, R3-IGF-I, ascorbic acid, heparin, and 10% human serum (control medium). Cells were used at passage 3 or earlier. Human brain pericytes (HBPs) (ACBRI 499; Cell Systems, Kirkland, WA) were used in a 1:4 ratio with HUVECs. First, HBPs were seeded into perfusion chambers (ibiTreat 6 lanes μ-Slide VI 0.4 Luer) at a concentration of 3×10^5 cells/mL. After cells were allowed to adhere for 2 h, HUVECs were seeded on top of them at a concentration of 1.2×10^6 cells/mL. After another 2 h of adherence, chambers were connected to a computer-controlled air pressure pump, which allowed for unidirectional perfusion of 15 mL of medium over the cell layers, generating a constant shear stress of 10 dyn/cm^2. The chamber and the reservoirs containing the medium were kept in an incubator at 37°C and 5% CO_2. Control medium was refreshed after 1 day to remove nonadherent cells, after which five conditions were tested: *1*) control medium; *2*) medium with 10% serum from a patient with diabetes (diabetic human serum [DHS]); *3*) DHS + 0.5 μmol/L atrasentan; *4*) DHS + 0.8 μmol/L heparanase inhibitor (OGT2115; Tocris, Bristol, UK); and *5*) DHS + 0.5 μmol/L atrasentan + 0.8 μmol/L heparanase inhibitor (n = 5). For each individual experiment, DHS was obtained from the blood of patients with diabetes and chronic hyperglycemia (HbA_{1c} >8.2% ([66 mmol/mol]). After 3 days, two lanes of cells were fixed with 4% paraformaldehyde in HBSS for 10 min, washed twice with HBSS, and blocked with 3% normal goat serum in HBSS for 30 min. Cells were incubated with an antibody against *N*-acetylated and *N*-sulfated heparan sulfate domains (clone 10E4, 10 μg/mL; Amsbio) or control IgM, both diluted in HBSS and incubated overnight at 4°C. Cells were subsequently washed and incubated with appropriate secondary antibodies and Hoechst 33528 (1/1,000) for 1 h, followed by tetramethylrhodamine-labeled wheat germ agglutinin (WGA) (1/100; Sigma-Aldrich) for 30 min. In the remaining lanes, cells were fixed with ice-cold methanol for 10 min to allow heparanase staining (HPA1, 1/20; InSight Biopharmaceuticals) or control IgG.

After being washed, cells were imaged using confocal microscopy and Leica Application Suite Advanced Fluorescence image software (Leica) to create image stacks. Luminal glycocalyx staining was analyzed using ImageJ software by first selecting the endothelial nuclear region. The thickness of the glycocalyx was quantified by calculating the distance from the half-maximum signal of the nuclear staining at the luminal side to the half-maximum signal at the luminal end of the staining in the *z*-direction. Luminal heparanase expression was quantified by selecting a similar endothelial nuclear region. The average intensity of every *z*-plane above the maximal intensity of the nucleus, until

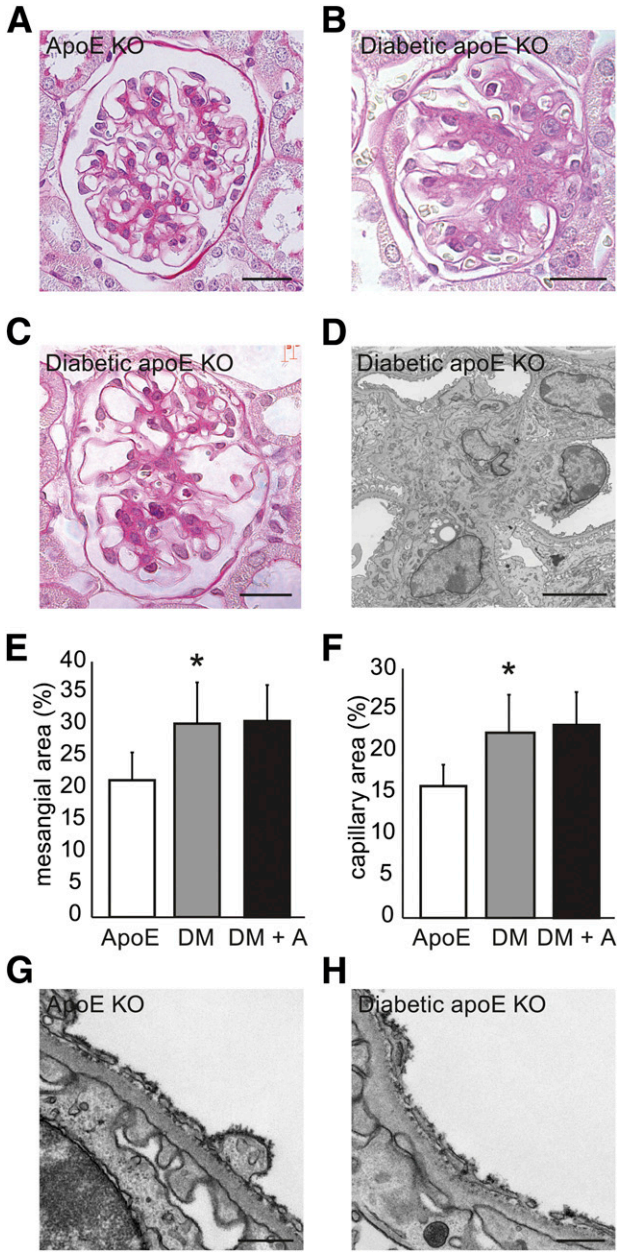

Figure 1—The diabetic apoE KO mouse model recapitulates the features of human diabetic nephropathy. *A*: The healthy glomerulus of a nondiabetic apoE KO mouse. Heterogeneous lesions in age-matched apoE KO mice 14 weeks after induction of diabetes with STZ show mesangial expansion (*B*), mesangiolysis (*C* and *D*), and, subsequently, glomerular hypertrophy, as quantified in *E* and *F*. *D*: TEM reveals a typical pathological process of mesangial foam cell formation and increased extracellular matrix deposition, resulting in decreased endothelial and mesangial cell interaction. TEM also shows differences in cationic ferritin coverage between nondiabetic (*G*) and diabetic (*H*) apoE KO mice. The occurrence of podocyte foot process effacement can be observed in *H*. Data are shown as mean ± SD (n = 8). *P < 0.05. Scale bars: 20 μm (*A–C*), 5 μm (*D*), 500 nm (*G* and *H*). ApoE, apoE KO mice; DM, diabetic apoE KO mice; DM + A, diabetic apoE KO mice + atrasentan.

the background level, was quantified and expressed as fold change compared with the control medium.

RNA Isolation and Quantitative RT-PCR Analysis

Murine glomerular endothelial cells from kidneys of eight mice per treatment group were isolated according to process described by Takemoto et al. (29). After removing CD45-positive cells with CD45 MicroBeads (Miltenyi Biotech, Germany), endothelial cells were selected by CD31 MicroBeads, according to the manufacturer's protocol. Total RNA was isolated from these cells or HUVECs using TRIzol (Invitrogen) and processed for real-time quantitative PCR using SYBR Green (Applied Biosystems). Human heparanase expression was identified with forward 5′-TCCTGCGTACCTGAGGTTTG-3′ and reverse 5′-CCATTCCAACCGTAACTTCTCCT-3′ primers. Relative mRNA expression was determined by normalizing to GAPDH.

Statistical Analysis

Data are presented as mean ± SD. Changes in albumin-to-creatinine ratios during treatment were analyzed using linear mixed-model regression analysis. This takes into account that samples taken over time from the same animal are not independent (SPSS Statistics, version 20; IBM). Differences in all other experiments with continuous variables were determined using the Student *t* test in SPSS. $P < 0.05$ was considered statistically significant.

RESULTS

Diabetic ApoE KO Mouse Model Recapitulates Features of Human Diabetic Nephropathy

Glomerular changes in diabetic apoE KO mice were determined 14 weeks after diabetes was induced and eating a cholesterol-enriched diet (0.15%). While glomeruli of nondiabetic apoE KO mice appeared healthy, with thin capillary loops and normal distribution of mesangial matrix, glomeruli of diabetic mice showed typical features of diabetic nephropathy, with heterogeneous lesions, including increased mesangial matrix accumulation and dilated capillaries. Computer-aided quantification of periodic acid Schiff– and trichrome-stained glomeruli revealed significantly larger capillary size and increased mesangial expansion (Fig. 1*A–C*, *E–F*).

Glomerular changes on an ultrastructural level were analyzed by exploiting large digital TEM images of full glomerular cross sections. Diabetes leads to thickening of the GBM (268 ± 20 nm in diabetic mice vs. 216 ± 17 nm in healthy mice; $P < 0.05$; $n = 3$), increased mesangial foam cell formation, and increased extracellular matrix, which results in decreased interaction between endothelial and mesangial cells (Fig. 1*D*). Endothelial fenestration was not affected by diabetes: 34.6 ± 9.0% of the endothelium in nondiabetic mice was fenestrated compared with 40.3 ± 7.2% in diabetic apoE KO mice ($n = 3$). Furthermore, an impaired glomerular filtration barrier was observed through focal podocyte foot process effacement and a decreased charge barrier, as shown by decreased cationic ferritin binding to the negatively charged glycocalyx (Fig. 1*G* and *H*).

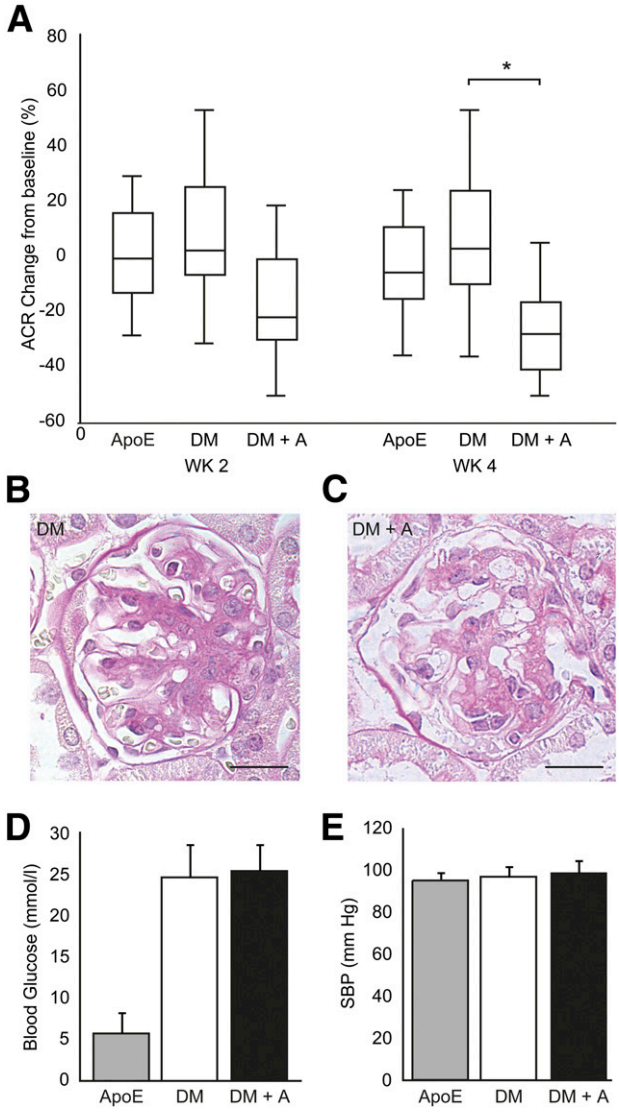

Figure 2—Atrasentan reduces albuminuria in diabetic apoE KO mice. *A*: Changes in urinary albumin-to-creatinine ratios (ACRs) from baseline to 4 weeks after treatment, indicated by percentage change from baseline. Data are shown as mean ± SD ($n = 19–23$). *$P < 0.01$. *B* and *C*: Glomerular morphology in diabetic apoE KO mice is not affected by treatment with atrasentan (DM + A) for 4 weeks compared with untreated diabetic apoE KO mice (DM). After treatment, no change in blood glucose concentrations (*D*) or systolic blood pressure (SBP) ($n = 8$) (*E*) is observed. Scale bars: 20 μm. ApoE, apoE KO mice.

Tubulointerstitial lesions were observed next to areas of glomerular damage in diabetic apoE KO mice, including focal tubulointerstitial extracellular matrix deposition and dilation of proximal and distal tubules. However, diabetes did not increase urinary KIM-1 excretion (1.09 ± 0.54 vs. 1.45 ± 0.48 ng/24 h; $n = 8$).

Atrasentan Reduces Albuminuria in Diabetic ApoE KO Mice

We tested the effect of 4 weeks of treatment with atrasentan (7.5 mg/kg/day) on albuminuria. At the end of the

intervention, body weight of treated mice was comparable to that of nontreated diabetic apoE KO mice (27.0 ± 2.4 g vs. 26.4 ± 2.6 g), which was lower than that of nondiabetic apoE KO mice (31.7 ± 2.8 g; $P < 0.05$). Nontreated diabetic apoE KO mice showed progressive albuminuria, which is in line with a parallel increase in urine production and albumin excretion (data not shown). Multiple comparisons demonstrate that treatment with atrasentan reduces progressive albuminuria by 26.0 ± 6.5% ($P < 0.01$) compared with control treatment (Fig. 2*A*). Renal morphology and capillary and mesangial areas were comparable to those in nontreated diabetic mice (23.3 ± 3.7% and 30.9 ± 6.0%, respectively; Figs. 1*E* and *F* and 2*B* and *C*). The number of podocytes stayed the same (data not shown), and at the current dose, treatment with atrasentan did not affect blood glucose concentrations (Fig. 2*D*) or blood pressure (Fig. 2*E*).

Atrasentan Restores Endothelial Glycocalyx Coverage

As a direct result of treatment of diabetic apoE KO mice with atrasentan, the negatively charged glomerular endothelial glycocalyx coverage was almost restored to control levels. This was visualized and quantified by glomerular endothelial cationic ferritin coverage (Fig. 3*A–C*) and lectin binding (Fig. 3*D–F*). Throughout the glomerular filtration barrier, cationic ferritin was present at the luminal endothelial cell surface, within the fenestrae, and directly underneath the endothelium, penetrating slightly into but never passing through the GBM. The presence of cationic ferritin in capillaries was used as an endogenous control: to control for possible bias introduced by perfusion staining, only capillaries that showed cationic ferritin on the surface of the endothelium or below the endothelium in the GBM were used for analyses. Diabetes results in less endothelial coverage (40.7 ± 3.2%) compared with that in nondiabetic apoE KO mice (83.6 ± 5.6%) (Fig. 3*C*). Treatment with atrasentan increases glomerular glycocalyx coverage back to the control (nondiabetic) state (81.0 ± 12.5%; $P < 0.05$).

In addition, nonperfused renal sections were stained with LEA, a lectin that binds β-(1,4)–linked *N*-acetylglucosamine residues to visualize the glycocalyx (13). Diabetes decreases the intraluminal lectin thickness from 1.62 ± 0.30 to 0.67 ± 0.17 μm ($P < 0.05$) (Fig. 3*F*). Treatment with atrasentan restores the intraluminal LEA thickness to 1.18 ± 0.25 μm ($P < 0.05$).

Atrasentan Increases NO Bioavailability

To confirm that activation of the ET_B receptor with ET-1 during the ET_A receptor blockade can induce the production of NO in the endothelium, endogenous renal NO bioavailability was measured using an in vivo NO-trapping method with Fe^{2+}-DETC complexes (26). A typical EPR

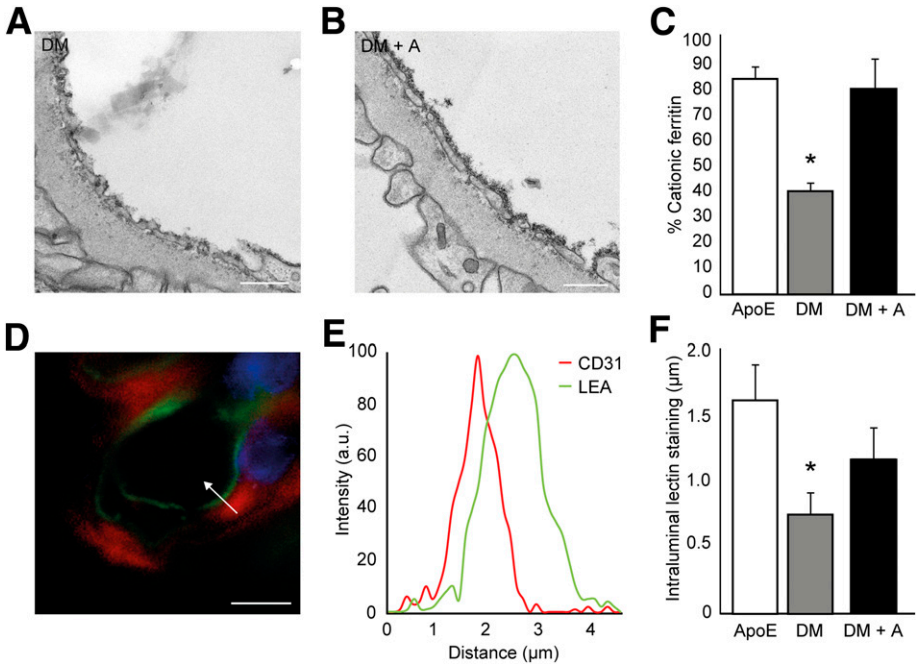

Figure 3—Atrasentan restores endothelial glycocalyx coverage. *A* and *B*: Representative TEM images of cationic ferritin bound to the negatively charged endothelial glycocalyx in glomeruli of diabetic (*A*) and atrasentan-treated diabetic (*B*) mice. *C*: Quantification of endothelial cationic ferritin coverage in capillary loops in three glomeruli of three mice, shown as the mean percentage of the total capillary length ± SD. *D*: Confocal fluorescent image of a glomerular capillary loop, stained for endothelial cells (CD31, red) and luminal glycocalyx (fluorescent-labeled LEA lectin, green). The arrow indicates the line of interest used in the intensity plot. *E*: Example of a fluorescence intensity plot depicting the area used for quantification of luminal glycocalyx thickness, which is determined by the distance of the CD31 peak to the half-maximum intensity of the LEA peak. *F*: Quantification of LEA thickness in capillary loops in three glomeruli of three mice. Data are shown as mean ± SD. Scale bars: 500 nm (*A* and *B*), 5 μm (*D*). *$P < 0.05$ compared with apoE KO mice (ApoE) and diabetic apoE KO mice + atrasentan (DM + A). a.u., arbitrary units; DM, diabetic apoE KO mice.

spectrum from renal mouse tissue is shown in Fig. 4*A*. It represents a yield of ~140 pmol paramagnetic ferrous MNIC in 246 mg of renal tissue from a diabetic apoE KO mouse after treatment with atrasentan. The renal NO yield in diabetic apoE KO mice increases from 0.29 ± 0.20 to 0.51 ± 0.15 pmol/mg (MNIC yield) (Fig. 4*B*). When diabetic mice are treated with atrasentan for 4 weeks, NO concentrations increase considerably to 0.74 ± 0.21 pmol/mg ($P < 0.05$).

Atrasentan Reduces Heparanase Expression and Shifts Macrophage Phenotype

A mechanism of reduced glycocalyx coverage is through increased breakdown of heparan sulfates, one of its major components, by heparanase. Diabetic mice show increased glomerular heparanase protein expression compared with nondiabetic apoE KO mice (39.3 ± 10.8% vs. 13.1 ± 9.2%; $P < 0.01$) (Fig. 5*A* and *C*). Treatment of diabetic mice with atrasentan effectively reduces glomerular heparanase protein expression to 19.4 ± 5.1% ($P < 0.01$). To explore the regulation of heparanase, mRNA expression in isolated glomerular endothelial cells was assessed. A strong transcriptional induction of heparanase expression was observed in the presence of diabetes (3.0 ± 1.2-fold; $P < 0.05$), which was reduced after treatment with atrasentan (1.6 ± 0.5), albeit not significantly ($P = 0.11$) (Supplementary Fig. 1). Inflammatory cells such as macrophages have been shown to increase heparanase activity by activation of secreted pro-heparanase by cathepsin-L (30,31). While the absolute number of macrophages remained equal between atrasentan-treated and nontreated diabetic mice (F4/80-positive cells: 2.15 ± 0.37 vs. 2.53 ± 0.42 per glomerulus, respectively), there was a shift from proinflammatory M1 macrophages toward regulatory, noninflammatory, CD206-positive M2 macrophages in atrasentan-treated mice (62.2 ± 11.1% vs. 44.8 ± 6.1%; $P < 0.01$), resulting in a distribution similar to that observed in nondiabetic apoE KO mice (64.8 ± 4.1%) (Fig. 5*A* and *B*). Concomitant with this shift in the macrophages phenotype and increased heparanase expression, we also observed increased cathepsin-L protein expression in diabetic apoE KO mice (27.3 ± 11.3% vs. 10.5 ± 2.8%; $P < 0.01$) and a reduction by atrasentan (10.1 ± 5.1%) (Fig. 5*A* and *D*). Notably, although cathepsin-L is more prominent in the tubular epithelium, glomerular F4/80-positive macrophages also colocalize with cathepsin-L expression (Supplementary Fig. 2).

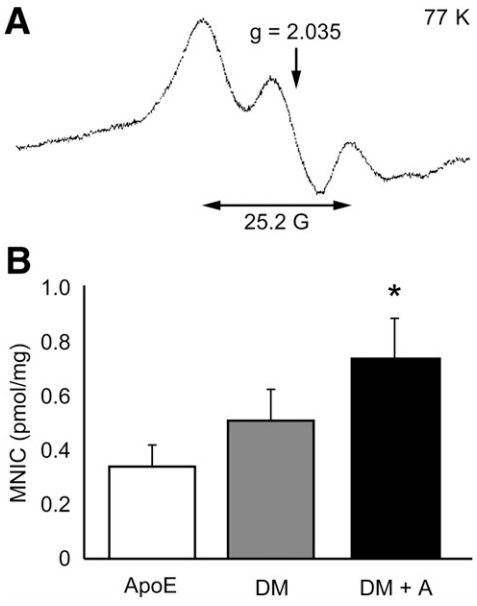

Figure 4—Atrasentan increases NO bioavailability. *A*: Example of the EPR spectrum of a frozen murine diabetic kidney sample after atrasentan treatment. The characteristic triplet structure of the MNIC (double-headed arrow) centers around g = 2.035 and represents the formation of local NO. *B*: Quantification of renal NO formation, shown as mean MNIC ± SD ($n = 8$ or 9). *$P < 0.05$ compared with diabetic apoE KO mice (DM). ApoE, apoE KO mice; DM + A, diabetic apoE KO mice + atrasentan.

Atrasentan Restores Glycocalyx Thickness on Endothelial Cells in a Diabetic Milieu by Reducing Heparanase

To further study our hypothesis that atrasentan can reduce endothelial heparanase expression under conditions of endothelial activation in diabetes and can subsequently increase glycocalyx thickness, we examined glycocalyx thickness on HUVECs in the presence of DHS and control human serum. HUVECs were cultured under flow (10 dyn/cm^2) for 4 days on top of a layer of HBPs to induce a quiescent endothelial phenotype and to resemble the in vivo cell–cell interactions that determine this endothelial phenotype. Under control conditions, these cells express a glycocalyx of 1.84 ± 0.36 μm, as shown with the lectin WGA (Fig. 6). To mimic the conditions present in diabetes, we exposed the endothelial cells to the serum of patients with poorly controlled diabetes. Importantly, while diabetes obviously is characterized by hyperglycemia, plasma from patients with diabetes contains a wide range of factors that may cause endothelial activation, including advanced glycation end products, chemokines such as MCP-1, and vasoactive peptides such as angiotensin and ET (32). To mimic these circumstances, cells were incubated for 3 days with a medium supplemented with the serum of patients with poorly controlled diabetes; consequently, glycocalyx thickness decreased to 1.12 ± 0.26 μm ($P < 0.05$). The addition of 0.5 μmol/L atrasentan to cells cultured in the presence of DHS restored glycocalyx thickness to 1.48 ± 0.19 μm ($P < 0.05$). The heparanase inhibitor OGT2115 also increased the glycocalyx thickness (1.38 ± 0.33 μm; $P < 0.05$). Adding both compounds simultaneously, however, had no synergetic effect (1.38 ± 0.33 μm; $P < 0.05$; data not shown). Staining with the antibody 10E4 against the *N*-acetylated and *N*-sulfated heparan sulfate domains, which was done to look more closely at the specific composition, showed results similar to the WGA staining (Fig. 6*A* and *B*).

To further test the involvement of heparanase in the modulation of the endothelial glycocalyx, we analyzed

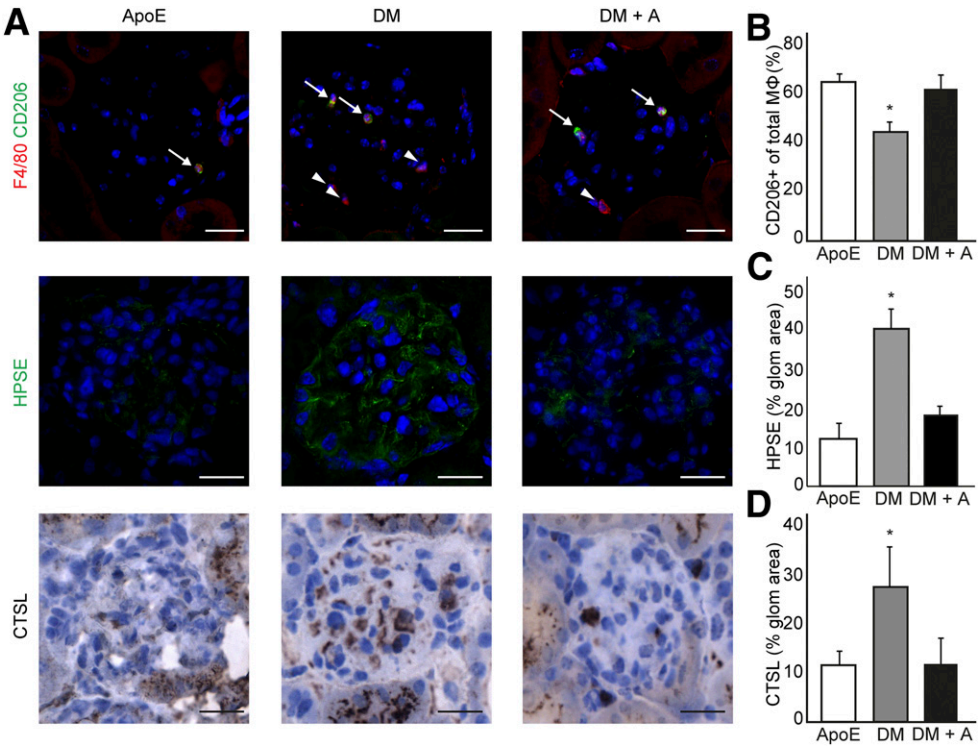

Figure 5—Atrasentan changes the glomerular M1-to-M2 macrophage ratio and reduces heparanase (HPSE) and cathepsin-L (CTSL) expression. *A*: Representative fluorescent images of glomerular F4/80 positive (arrowheads, top row) and F4/80-CD206 double-positive macrophages (arrows, top row), HPSE expression (middle row), and CTSL expression (bottom row) in apoE KO mice (ApoE), nontreated diabetic apoE KO mice (DM), and diabetic apoE KO mice treated with atrasentan (DM + A). Scale bars: 20 μm. Quantification of percent CD206-positive cells per total macrophage cell count (*B*) and percent HPSE- (*C*) and CTSL-positive (*D*) area per glomerulus. Data are shown as mean ± SD (n = 8). *P < 0.01 compared with ApoE and DM + A. glom, glomerular.

heparanase gene expression and heparanase protein presence at the luminal surface of the endothelial cells (Fig. 6*C*). In agreement with the in vivo studies, incubation with DHS for 3 days induced a 1.63 ± 0.27-fold increase in luminal protein expression, which was paralleled by a 1.46 ± 0.28-fold increase in mRNA expression compared with incubation in nondiabetic serum ($P < 0.05$). Supplementation of these cells by 0.5 μmol/L atrasentan cultured in the presence of DHS normalized both luminal heparanase protein expression, as well as mRNA expression (to 1.19 ± 0.23-fold and 1.10 ± 0.11-fold compared with control, respectively). The heparanase inhibitor decreased luminal expression of heparanase 1.25 ± 0.22-fold ($P < 0.05$), but not gene expression (1.2 ± 0.46-fold), and there was no amplification of the effect of atrasentan.

DISCUSSION

In this study selective ET_A receptor blockade in diabetic nephropathy is associated with almost complete restoration of glomerular endothelial glycocalyx dimensions toward control values and a reduction of albuminuria. Especially, the profound reduction of albuminuria occurs in the absence of any changes in systemic blood pressure and metabolic activators, such as high glucose concentrations. Both the in vivo data as well as the mechanistic studies in vitro show that atrasentan is capable of reducing heparanase expression in the presence of a diabetic milieu. This study provides a new mechanism of action for ongoing clinical studies with ET_A receptor blockers in diabetic nephropathy, where similar strong reductions in proteinuria were observed in the presence of only minor hemodynamic effects (11).

There has been controversy with respect to both the mechanism of albuminuria and the possible consequences of albuminuria in diabetic nephropathy. Most experimental data point to size selectivity of the glomerular filter. The glomerular glycocalyx, through its mesh of glycosaminoglycans and associated proteins, constitutes a size-selective hydrogel that covers the surface and in particular the fenestrae (33). Disruption of this structure by enzymatic treatment, or more recently by endothelial deletion of the hyaluronan synthase 2 gene, has been shown to result in albuminuria (13,34). Moreover, the high heparan sulfate content and the presence of sialylated proteins may give the endothelial surface a net negative charge, thus possibly further modulating the sieving of macromolecules. Since diabetes is associated with endothelial dysfunction and reduced systemic glycocalyx dimensions (12,15), restoration of endothelial function and glycocalyx dimensions may thus prevent albuminuria. Such a therapy

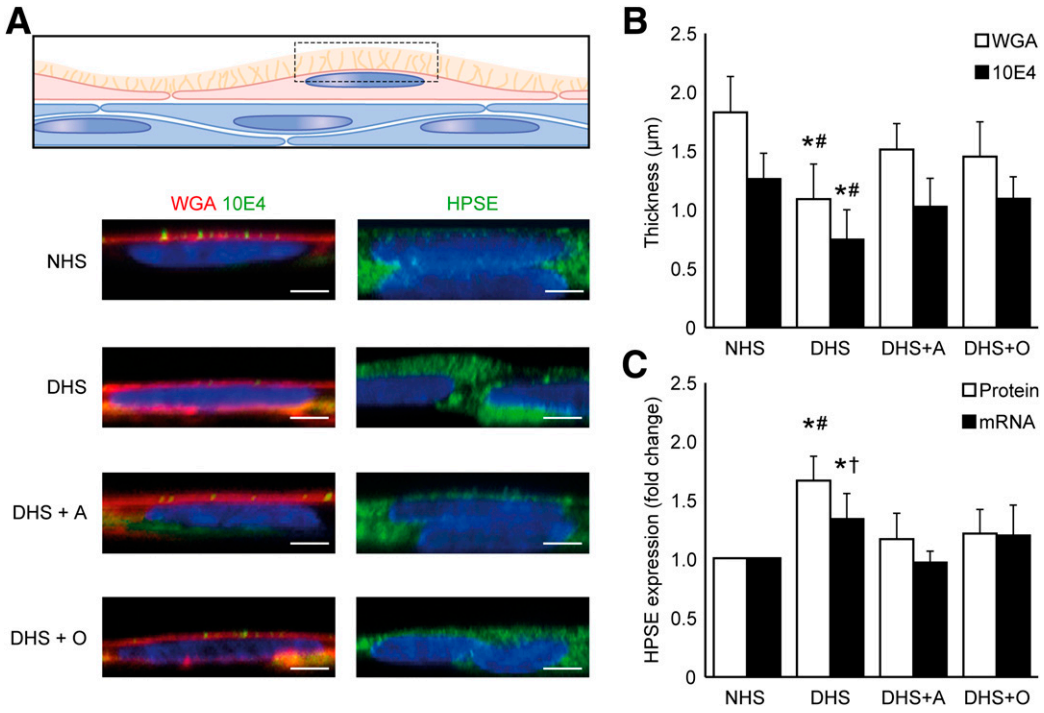

Figure 6—Atrasentan restores glycocalyx thickness on HUVECs. *A*: Schematic showing the area of interest for quantification (top, dotted line). Confocal fluorescent *z*-axis average-intensity projections of HUVECs cultured on top of HBPs under laminar flow for 4 days is shown on the bottom. On the left are intensities of WGA lectin (red) and specific anti–heparan sulfate staining (10E4; green). On the right is anti-heparanase (HPSE) staining. *B*: Glycocalyx thickness is quantified by estimating the distance from the half-maximum signal of the nuclear staining to the half maximum signal at the luminal end of WGA and 10E4 staining. *C*: Endothelial HPSE protein and mRNA expression are shown as relative to the control (normal human serum [NHS]). Protein expression is quantified as average intensity staining in the area of interest (*A*). Data are shown as mean ± SD ($n = 4$ or 5). *$P < 0.05$ compared with NHS. #$P < 0.05$ versus each treatment. †$P < 0.05$ versus atrasentan treatment. Scale bars: 10 μm. DHS + A = DHS + 5 μmol/L atrasentan; DHS + O = DHS + HPSE inhibitor (OGT2115).

would be meaningful in the setting of diabetes, where chronic exposure of the glomerular and tubular endothelium to glycated albumin has been shown to induce epithelial inflammation and set the stage for tubulointerstitial disease (35).

To corroborate the beneficial effects of atrasentan on endothelial function, we used paramagnetic ferrous MNIC spin-trap measurements; this model allows for quantitative measurements of the amount of NO molecules produced locally (27). Atrasentan increased NO production at the renal tissue level (26), thus confirming endothelial ET_B receptor stimulation and restoration of endothelial function (36), despite the presence of diabetes.

To further address the mechanism behind the beneficial effects of atrasentan on heparanase reduction and its effect on endothelial glycocalyx dimensions, we also studied the effect of atrasentan on the endothelial glycocalyx in vitro. Because the glycocalyx composition is critically dependent upon shear, the cellular environment, and endothelial function, we used an experimental setup in which endothelial cells were exposed to laminar flow and cultured on top of pericytes, meant to mimic as closely as possible the in vivo situation. Endothelial cells show a remarkable heterogeneity throughout the vascular tree and may therefore differ in their response to injury (37,38). Despite this heterogeneity, HUVECs are capable of expressing heparanase (39), and in this model, adding DHS—thereby mimicking the diabetic milieu—increased endothelial heparanase expression. Heparanase is the main enzyme that can break down heparan sulfate side chains of glycosaminoglycans, and consequently glycocalyx thickness is reduced. In line with our observations in mice, atrasentan reduced heparanase expression through transcriptional regulation and restored the reduction of glycocalyx thickness in the presence of DHS. Atrasentan was as effective as a heparanase inhibitor, and the heparanase inhibitor did not amplify the effect of atrasentan, indicating that direct modulation of endothelial heparanase expression may be a mechanism by which atrasentan restores the glycocalyx.

Atrasentan has been studied previously in other diabetic animal models. In a STZ-induced diabetic rat model atrasentan reduced the onset of albuminuria, independent of changes in blood pressure (7,40). Using the same model as in this study, avosentan, another ET_A selective blocker, was also shown to have strong antialbuminuric effects (17). Similar to our study, this was accompanied by anti-inflammatory effects, such as reduced influx of renal macrophages and additional decreased plasma concentrations of the

inflammatory markers MCP-1 and soluble intracellular adhesion molecule-1. Such anti-inflammatory effects may have contributed further to the reduction in heparanase expression that was observed in the diabetic mice, since infiltrating monocytes have been shown to contribute to the activation of secreted proheparanase (41). This is supported by our observations that atrasentan reduced glomerular expression of cathepsin-L, the enzyme that activates proheparanase; cathepsin-L expression colocalized with inflammatory glomerular macrophages.

Sitaxsentan, another ET_A receptor blocker, was shown to reduce podocyte loss in adriamycin-induced nephropathy (42). However, we did not observe a change in podocyte numbers in our model. Furthermore, we did not see changes in systemic blood pressure during atrasentan treatment. However, a reduction in glomerular capillary pressure cannot be ruled out as a possible mechanism to explain the beneficial effects on glomerular ultrastructure and glomerular endothelial glycocalyx function, particularly because micropuncture studies in rats have demonstrated the presence of increased glomerular capillary pressure in models of STZ-induced diabetes (43). Unfortunately, this technology cannot be applied to mice.

While our model studied only the short-term effects of atrasentan in already developed diabetic nephropathy, it would, of course, be relevant to know whether prolonged restoration of the glomerular glycocalyx also results in restoration of the cellular morphology or the prevention of (further) renal lesions. Both the effectiveness in preventing albuminuria as well as the fact that the glomerular glycocalyx functions as a molecular scaffold that modulates renal inflammation makes this question pertinent. Unfortunately, the long duration of the model, which was required to faithfully replicate changes seen in human diabetic nephropathy, precluded such follow-up studies in STZ-treated animals. This does not, however, detract from the fact that this study corroborates the rationale for the clinical use of ET_A selective receptor blockade in diabetic nephropathy; given the systemic nature of loss of the glycocalyx in diabetes, it also provides a mechanism of action that can be monitored noninvasively (44) in patients before and during treatment.

Acknowledgments. The authors thank E. Bouwman (Department of Inorganic Chemistry, Leiden University) for the use of the EPR facilities.

Funding. This study was supported by the Dutch Kidney Foundation (Glycoren Consortium grant no. CP09.03) and by AbbVie (grant no. REN-11-0026).

Duality of Interest. No potential conflicts of interest relevant to this article were reported.

Author Contributions. M.G.S.B. designed the experiments, researched and analyzed the data, and wrote and revised the manuscript. M.C.A., A.K., M.J.C.D., D.H.L., and E.v.F. acquired and interpreted the data and critically revised the manuscript. J.v.d.V., A.J.K., A.J.v.Z., and H.-J.G. critically revised the manuscript for important intellectual content. B.M.v.d.B. and T.J.R. conceived, designed, and supervised the study and critically revised the manuscript. T.J.R. is the guarantor of this work and, as such, had full access to all the data in the study and takes responsibility for the integrity of the data and the accuracy of the data analysis.

Prior Presentation. Parts of this study were presented in abstract form at the American Society of Nephrology Kidney Week, Philadelphia, PA, 11–16 November 2014.

References

1. U.S. Renal Data System. *Annual Data Report: Atlas of Chronic Kidney Disease and End-Stage Renal Disease in the United States*. Bethesda, MD, National Institutes of Health, National Institute of Diabetes and Digestive and Kidney Diseases, 2012

2. Hocher B, Thöne-Reineke C, Rohmeiss P, et al. Endothelin-1 transgenic mice develop glomerulosclerosis, interstitial fibrosis, and renal cysts but not hypertension. J Clin Invest 1997;99:1380–1389

3. Barton M. Therapeutic potential of endothelin receptor antagonists for chronic proteinuric renal disease in humans. Biochim Biophys Acta 2010;1802:1203–1213

4. Kohan DE, Pollock DM. Endothelin antagonists for diabetic and non-diabetic chronic kidney disease. Br J Clin Pharmacol 2013;76:573–579

5. Kohan DE, Pritchett Y, Molitch M, et al. Addition of atrasentan to renin-angiotensin system blockade reduces albuminuria in diabetic nephropathy. J Am Soc Nephrol 2011;22:763–772

6. Kohan DE, Barton M. Endothelin and endothelin antagonists in chronic kidney disease. Kidney Int 2014;86:896–904

7. Sasser JM, Sullivan JC, Hobbs JL, et al. Endothelin A receptor blockade reduces diabetic renal injury via an anti-inflammatory mechanism. J Am Soc Nephrol 2007;18:143–154

8. Edwards RM, Pullen M, Nambi P. Activation of endothelin ET_B receptors increases glomerular cGMP via an L-arginine-dependent pathway. Am J Physiol 1992;263:F1020–F1025

9. Hirata Y, Emori T, Eguchi S, et al. Endothelin receptor subtype B mediates synthesis of nitric oxide by cultured bovine endothelial cells. J Clin Invest 1993;91:1367–1373

10. Nakano D, Pollock JS, Pollock DM. Renal medullary ET_B receptors produce diuresis and natriuresis via NOS1. Am J Physiol Renal Physiol 2008;294:F1205–F1211

11. de Zeeuw D, Coll B, Andress D, et al. The endothelin antagonist atrasentan lowers residual albuminuria in patients with type 2 diabetic nephropathy. J Am Soc Nephrol 2014;25:1083–1093

12. Meuwese MC, Broekhuizen LN, Kuikhoven M, et al. Endothelial surface layer degradation by chronic hyaluronidase infusion induces proteinuria in apolipoprotein E-deficient mice. PLoS One 2010;5:e14262

13. Dane MJ, van den Berg BM, Avramut MC, et al. Glomerular endothelial surface layer acts as a barrier against albumin filtration. Am J Pathol 2013;182:1532–1540

14. van den Hoven MJ, Rops AL, Bakker MA, et al. Increased expression of heparanase in overt diabetic nephropathy. Kidney Int 2006;70:2100–2108

15. Nieuwdorp M, Mooij HL, Kroon J, et al. Endothelial glycocalyx damage coincides with microalbuminuria in type 1 diabetes. Diabetes 2006;55:1127–1132

16. Opgenorth TJ, Adler AL, Calzadilla SV, et al. Pharmacological characterization of A-127722: an orally active and highly potent ET_A-selective receptor antagonist. J Pharmacol Exp Ther 1996;276:473–481

17. Watson AM, Li J, Schumacher C, et al. The endothelin receptor antagonist avosentan ameliorates nephropathy and atherosclerosis in diabetic apolipoprotein E knockout mice. Diabetologia 2010;53:192–203

18. Lassila M, Jandeleit-Dahm K, Seah KK, et al. Imatinib attenuates diabetic nephropathy in apolipoprotein E-knockout mice. J Am Soc Nephrol 2005;16:363–373

19. Meyrelles SS, Peotta VA, Pereira TM, Vasquez EC. Endothelial dysfunction in the apolipoprotein E-deficient mouse: insights into the influence of diet, gender and aging. Lipids Health Dis 2011;10:211

20. Lassila M, Seah KK, Allen TJ, et al. Accelerated nephropathy in diabetic apolipoprotein e-knockout mouse: role of advanced glycation end products. J Am Soc Nephrol 2004;15:2125–2138
21. Tran TN, Eubanks SK, Schaffer KJ, Zhou CY, Linder MC. Secretion of ferritin by rat hepatoma cells and its regulation by inflammatory cytokines and iron. Blood 1997;90:4979–4986
22. Faas FG, Avramut MC, van den Berg BM, Mommaas AM, Koster AJ, Ravelli RB. Virtual nanoscopy: generation of ultra-large high resolution electron microscopy maps. J Cell Biol 2012;198:457–469
23. Avasthi PS, Koshy V. The anionic matrix at the rat glomerular endothelial surface. Anat Rec 1988;220:258–266
24. Austyn JM, Gordon S. F4/80, a monoclonal antibody directed specifically against the mouse macrophage. Eur J Immunol 1981;11:805–815
25. Ezekowitz RA, Gordon S. Alterations of surface properties by macrophage activation: expression of receptors for Fc and mannose-terminal glycoproteins and differentiation antigens. Contemp Top Immunobiol 1984;13:33–56
26. Vanin AF, Huisman A, van Faassen EE. Iron dithiocarbamate as spin trap for nitric oxide detection: pitfalls and successes. Methods Enzymol 2002;359:27–42
27. van Faassen EE, Koeners MP, Joles JA, Vanin AF. Detection of basal NO production in rat tissues using iron-dithiocarbamate complexes. Nitric Oxide 2008;18:279–286
28. Berliner LJ, Fujii H. In vivo spin trapping of nitric oxide. Antioxid Redox Signal 2004;6:649–656
29. Takemoto M, Asker N, Gerhardt H, et al. A new method for large scale isolation of kidney glomeruli from mice. Am J Pathol 2002;161:799–805
30. Garsen M, Rops AL, Rabelink TJ, Berden JH, van der Vlag J. The role of heparanase and the endothelial glycocalyx in the development of proteinuria. Nephrol Dial Transplant 2014;29:49–55
31. Goldberg R, Rubinstein AM, Gil N, et al. Role of heparanase-driven inflammatory cascade in pathogenesis of diabetic nephropathy. Diabetes 2014;63:4302–4313
32. Eelen G, de Zeeuw P, Simons M, Carmeliet P. Endothelial cell metabolism in normal and diseased vasculature. Circ Res 2015;116:1231–1244
33. Rostgaard J, Qvortrup K. Electron microscopic demonstrations of filamentous molecular sieve plugs in capillary fenestrae. Microvasc Res 1997;53:1–13
34. van den Berg BM, Boels MGS, Avramut MC, et al. Genetic deletion of endothelial hyaluronan synthase 2 results in glomerular injury and albuminuria (Abstract). J Am Soc Nephrol 2014;25:29A
35. Nauta FL, Boertien WE, Bakker SJ, et al. Glomerular and tubular damage markers are elevated in patients with diabetes. Diabetes Care 2011;34:975–981
36. Tsukahara H, Ende H, Magazine HI, Bahou WF, Goligorsky MS. Molecular and functional characterization of the non-isopeptide-selective ETB receptor in endothelial cells. Receptor coupling to nitric oxide synthase. J Biol Chem 1994;269:21778–21785
37. Yuan L, Chan GC, Beeler D, et al. A role of stochastic phenotype switching in generating mosaic endothelial cell heterogeneity. Nat Commun 2016;7:10160
38. Ligresti G, Nagao RJ, Xue J, et al. A novel three-dimensional human peritubular microvascular system. J Am Soc Nephrol. 11 December 2015 [Epub ahead of print] DOI:10.1681/ASN.2105070747
39. Godder K, Vlodavsky I, Eldor A, Weksler BB, Haimovitz-Freidman A, Fuks Z. Heparanase activity in cultured endothelial cells. J Cell Physiol 1991;148:274–280
40. Saleh MA, Boesen EI, Pollock JS, Savin VJ, Pollock DM. Endothelin receptor A-specific stimulation of glomerular inflammation and injury in a streptozotocin-induced rat model of diabetes. Diabetologia 2011;54:979–988
41. Fiebiger E, Maehr R, Villadangos J, et al. Invariant chain controls the activity of extracellular cathepsin L. J Exp Med 2002;196:1263–1269
42. Buelli S, Rosanò L, Gagliardini E, et al. β-Arrestin-1 drives endothelin-1-mediated podocyte activation and sustains renal injury. J Am Soc Nephrol 2014;25:523–533
43. Qiu C, Samsell L, Baylis C. Actions of endogenous endothelin on glomerular hemodynamics in the rat. Am J Physiol 1995;269:R469–R473
44. Dane MJ, Khairoun M, Lee DH, et al. Association of kidney function with changes in the endothelial surface layer. Clin J Am Soc Nephrol 2014;9:698–704